Available online at www.sciencedirect.com
SCIENCE DIRECT®

Journal of the European Ceramic Society 24 (2004) 3245–3249

www.elsevier.com/locate/jeurceramsoc

Effect of sintering atmosphere on the mechanical properties of liquid-phase-sintered SiC

A.L. Ortiz[a], A. Muñoz-Bernabé[b], O. Borrero-López[a], A. Domínguez-Rodríguez[b], F. Guiberteau[a,*], N.P. Padture[c]

[a]*Departamento de Electrónica e Ingeniería Electromecánica, Escuela de Ingenierías Industriales, Universidad de Extremadura, 06071 Badajoz, Spain*

[b]*Departamento de Física de la Materia Condensada, Facultad de Física, Universidad de Sevilla, 1065-41080 Seville, Spain*

[c]*Department of Metallurgy and Materials Science Engineering, Institute of Materials Science, University of Connecticut, Storrs, CT 06269-3136, USA*

Received 24 September 2003; accepted 25 October 2003

Abstract

It has been demonstrated that sintering atmosphere (Ar or N_2) exerts a strong influence on the microstructural evolution in liquid-phase-sintered (LPS) SiC with oxide additives. N_2-atmosphere sintering (β-SiC stating powders) results in LPS SiC with equiaxed-grained microstructures, and "strong" and more viscous nitrogen-containing intergranular phase. In contrast, Ar-atmosphere sintering results in LPS SiC with elongated-grained microstructures, and "weak" and less viscous intergranular phase. This has a profound effect on the room- and high-temperature mechanical properties of LPS SiC. N_2–LPS SiC is less "quasi-ductile" under Hertzian indentation, harder, and more brittle. In contrast, Ar–LPS SiC is more "quasi-ductile", softer, and tougher. At high temperature, N_2–LPS SiC is more deformation-resistant, stronger, but fails at lower strains. Ar–LPS SiC, on the other hand, has lower deformation resistance, lower ultimate compressive strength, but higher strain-to-failure. This contrast in the mechanical properties of the two materials is discussed in the context of the microstructures they possess.

Keywords: Indentation; Liquid-phase sintering; Mechanical properties; Microstructures; SiC

1. Introduction

Liquid-phase-sintered (LPS) silicon carbide (SiC) with oxide additives (Al_2O_3, Y_2O_3) has a remarkable combination of mechanical, thermal, and chemical properties, which makes this material a promising structural ceramic.[1–9] Steady progress has been made over the past decade in understanding the microstructural evolution in LPS SiC, and the microstructural influence on the mechanical properties of LPS SiC.[2–8,10–17] Recently, it has been demonstrated that nitrogen (incorporated using additive or sintering atmosphere) exerts a strong influence on the microstructural evolution, and the attendant mechanical properties of LPS SiC.[8,18,19] In particular, it has been demonstrated that sintering LPS SiC in N_2 atmosphere (β-SiC starting powders), suppresses the $\beta \rightarrow \alpha$ phase transformation, which otherwise goes to completion in Ar atmosphere. Consequently, the microstructures of LPS SiC sintered in N_2 atmosphere are equiaxed.[19] More importantly, N_2-atmosphere sintering of LPS SiC leads to the incorporation of nitrogen in the intergranular phase making it highly refractory. This results in coarsening-resistant microstructures that have very high internal friction—highly desirable attributes in a high-temperature structural ceramic.[19] The objective of this study was to elucidate further the effect of sintering atmosphere (Ar or N_2) on the room- and high-temperature properties of LPS SiC.

2. Experimental

2.1. Processing

The processing procedure used here was identical to the one employed in the earlier studies.[16,19] Briefly, two powder batches were individually prepared, each containing

* Corresponding author.
E-mail address: guiberto@unex.es (F. Guiberteau).

0955-2219/$ - see front matter © 2003 Elsevier Ltd. All rights reserved.
doi:10.1016/j.jeurceramsoc.2003.10.047

73.86 wt.% β-SiC (Ultrafine SiC, Ibiden Corp., Japan) plus 14.92 wt.% Al_2O_3 (AKP-30, Sumitomo Chemical Company, New York, NY) and 11.22 wt.% Y_2O_3 (Fine Grade, H.C. Starck Inc., Newton, MA) to result in 20 vol.% yttrium aluminum garnet (YAG) in the LPS SiC specimens. From each of the powder batches several pellets (approx. 10 g each) were uniaxially pressed in a steel die (25 mm diameter) at 50 MPa pressure. All pellets were subsequently cold-isostatically pressed (CP360, AIP, Columbus, OH) at a pressure of 350 MPa. Individual pellets were embedded in powder beds inside graphite crucibles with screwable lids. The pellets were sintered at 1950 °C for 1 h in either flowing Ar or N_2 gas atmospheres, and will referred to as Ar–LPS SiC and N_2–LPS SiC, respectively. (See Refs. 16 and 19 for processing details.)

2.2. Mechanical properties characterization

2.2.1. Room temperature

Hertzian and Vickers indentation tests were performed on both Ar–LPS SiC and N_2–LPS SiC, using methods described elsewhere.[20,21] Briefly, bar specimens ($20\times2.5\times2.5$ mm^3) of each material were machined out of the sintered discs, and the cross-sectional long faces (20×2.5 mm^2) were polished to a 1 μm finish using routine ceramographic techniques. In the case of Hertzian indentation, the polished surfaces were sputter-coated with gold prior to indentation. Hertzian indentations were made on those surfaces normally in a universal testing machine (Model 5565, Instron, Canton, MA) at constant crosshead speed (5 μm min^{-1}) over a load range $P = 15$–3500 N, using tungsten carbide spheres of radii $r = 1.98$, 3.18, 4.76, 7.94, and 12.7 mm, in air. The contact radius a for each indentation was measured from residual impressions left in the gold coating using an optical microscope in Nomarski interference contrast mode (Nikon Epiphot 300, Tokyo, Japan). Two indentations were performed for each material, per loading condition and indenter ball size. This enabled us to evaluate the indentation pressure ($p_0 = P/\pi a^2$) and indentation strain (a/r). The Hertzian indentation test provides fundamental information about the elastic and plastic deformation properties at room temperature of otherwise brittle ceramics, information not attainable generally in more conventional mechanical tests.[22,23]

Vickers indentation tests were performed on both Ar–LPS SiC and N_2–LPS SiC polished specimens, in order to evaluate their hardness (H) and toughness (K_{IC}). All Vickers indentation tests were performed in air using a hardness tester (Model MV-1, Matsuzawa, Tokyo, Japan) equipped with Vickers diamond pyramid, with maximum load (P) of 98 N, indentation load rate of 40 μm s^{-1} and dwell time of 20 s. Ten separate indentations were performed for each material. Subsequently, the tested surface was gold-coated for observation in the optical microscope. The length of the diagonal ($2d$) of the residual impression and the total length of the surface trace of the radial cracks ($2c$) were then measured in the optical microscope (using Nomarski interference contrast). The hardness and the toughness were determined using standard formulae.[21]

2.2.2. (B) High temperature

Specimens ($5\times2.5\times2.5$ mm^3) were machined out of the sintered discs of the two materials, and all specimen faces were polished to a 3 μm finish (several specimens were tested prior to polishing; no differences in the mechanical behaviour between the machined and polished specimens were observed). Uniaxial compression deformation tests were performed in air at 1400 °C using an universal testing machine (Model 1185, Instron, Canton MA), with the square faces (2.5×2.5 mm^2) normal to the loading axis. The specimen was sandwiched between two solid-state-sintered SiC platens in order to avoid damage to the Al_2O_3 push rods. A constant crosshead of 5 μm min^{-1} was used, corresponding to an initial strain rate ($\dot{\varepsilon}$) of 1.7×10^{-5} s^{-1}. Prior to testing, the specimens were heated to 1400 °C with a heating rate of 600 °C h^{-1} under 40 N preload and soaked for 1 h in order to ensure thermal equilibrium conditions. The load–displacement data was recorded continuously, and it was analyzed in terms of the engineering stress (σ_e) and % engineering strain (%ε_e).

2.3. Microstructural characterization

The microstructure data (density, grain length L, grain width D) for Ar–LPS SiC and N_2–LPS SiC specimens were obtained from the earlier studies on the same materials.[16,19] Microstructural damage in both Ar–LPS SiC and N_2–LPS SiC after the high-temperature testing was observed using a scanning electron microscope or SEM (Model XL30, Philips Research Laboratories, Eindhoven, The Netherlands). Prior to SEM observation, the specimen surfaces were plasma-etched[16,19] and sputter-coated with gold.

3. Results

Fig. 1(a) and 1(b) are SEM micrographs showing the microstructures of Ar–LPS SiC and N_2–LPS SiC, respectively, from the earlier studies.[16,19] The scale of the SiC grains in the two materials is nominally the same (average $D \sim 0.6$ μm), however, the aspect ratio of the SiC grains in Ar-LPS SiC is higher ($L/D \sim 2.0$) than that in the N_2-LPS SiC ($L/D \sim 1.4$).[16,19] Both materials have densities in excess of 98% of the theoretical limit of 3.484 g cm^{-3}.

Fig. 2 is a plot of the Hertzian indentation pressure–strain data obtained for Ar–LPS SiC and N_2–LPS SiC;

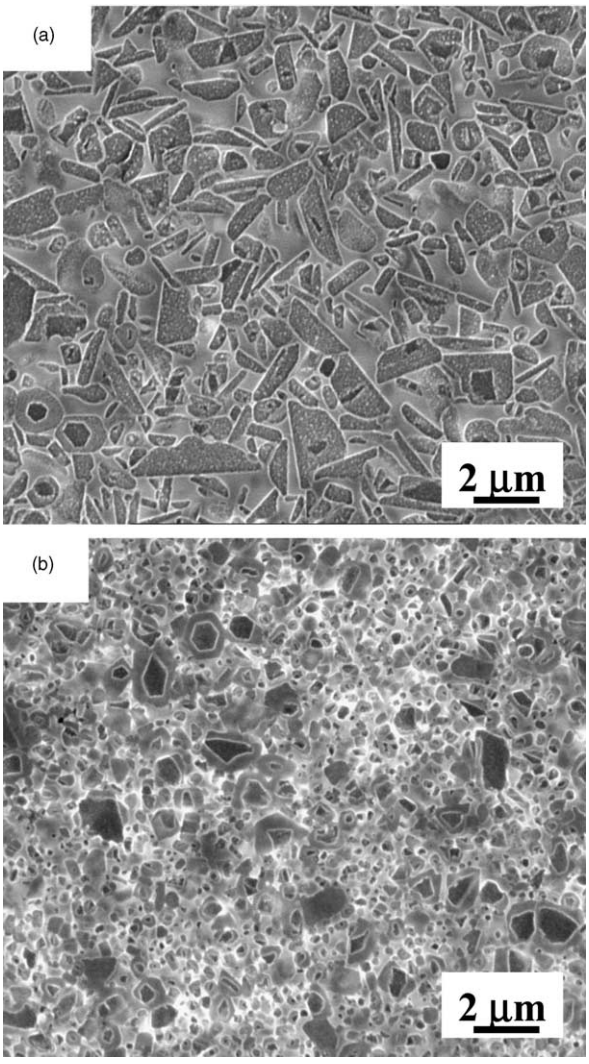

Fig. 1. SEM micrographs of plasma-etched microstructures of LPS SiC processed in (a) Ar atmosphere, and (b) N_2 atmosphere. Dark regions are SiC grains and light region is the intergranular phase. Core-shell substructure within SiC grains is visible in the micrographs, due to differential plasma-etching after Ref. [16].

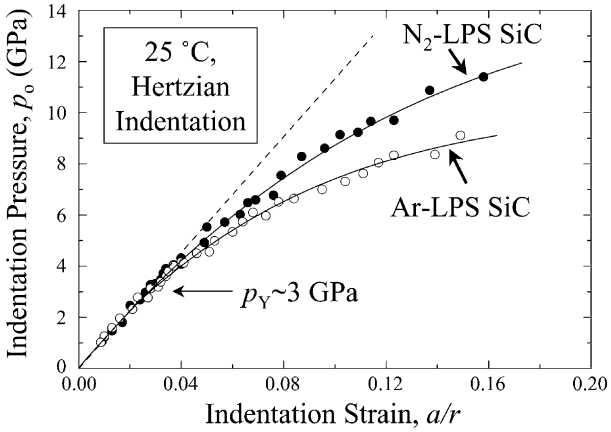

Fig. 2. Indentation pressure–strain curves at room-temperature for single-cycle Hertzian contacts in LPS SiC processed in Ar (open circles) and in N_2 (closed circles) atmospheres. The solid curves through the data are empirical fits. The dashed line represents the Hertzian elastic response.

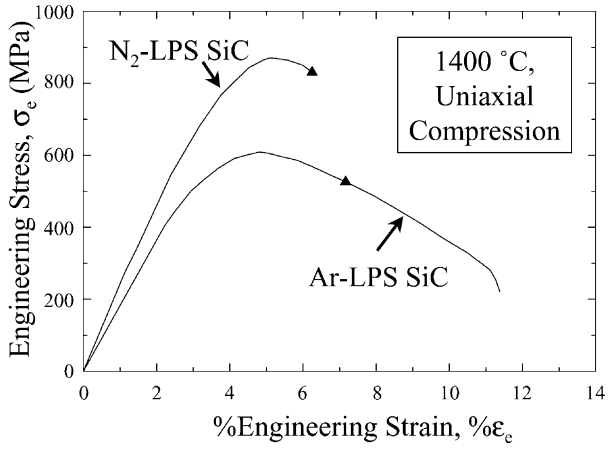

Fig. 3. Engineering stress–% engineering strain curves for uniaxial compression deformation at 1400 °C in LPS SiC processed in Ar and N_2 atmospheres. The triangles denote the stress–strain conditions at which the specimens were observed in the SEM.

the solid curves through the data are empirical fits. In Fig. 2 the pressure–strain curves overlap in their linear stretches, indicating a common elastic response. The dashed line represents the fit for a perfectly linear-elastic behaviour, from where an elastic modulus of $E = 382 \pm 4$ GPa is calculated. This compares favorably with the elastic modulus of $E = 396$ GPa calculated using rule-of-mixtures ($0.8E_{SiC} + 0.2E_{YAG}$), with $E_{SiC} = 425$ GPa[21] and $E_{YAG} = 280$ GPa.[24] Fig. 2 also shows that the curves bend away from the linear-elastic behaviour at pressures $p_Y \sim 3$ GPa, which constitutes the onset of plastic deformation. However, Ar–LPS SiC exhibits enhanced "quasi-ductile" behavior compared with N_2–LPS SiC.

The Vickers hardness measured for Ar–LPS SiC was found to be lower ($H = 17.6 \pm 0.3$ GPa) than that for N_2–LPS SiC ($H = 20.7 \pm 0.6$ GPa). In contrast, the Vickers-indentation toughness of Ar–LPS SiC was higher ($K_{IC} = 3.3 \pm 0.1$ MPa.m$^{1/2}$) compared with that of N_2–LPS SiC ($K_{IC} = 2.2 \pm 0.1$ MPa.m$^{1/2}$).

Fig. 3 shows representative engineering stress–% engineering strain (compression) curves obtained for Ar–LPS SiC and N_2–LPS SiC at 1400 °C. The following observations can be made from Fig. 3: (i) Ar–LPS SiC and N_2–LPS SiC both deform elastically up to strain $\%\varepsilon_e \sim 1.8$, (ii) the ultimate compression strength (peak stress) of N_2–LPS SiC ($\sigma_{UCS} \sim 870$ MPa) is significantly higher than that of Ar–LPS SiC ($\sigma_{UCS} \sim 630$ MPa), and (iii) the total strain at catastrophic failure is significantly higher for Ar–LPS SiC ($\%\varepsilon_F \sim 11.4$) compared with N_2–LPS SiC ($\%\varepsilon_F \sim 6$). In both materials, catastrophic failure is characterized by a single crack spanning the entire specimen along the loading axis.

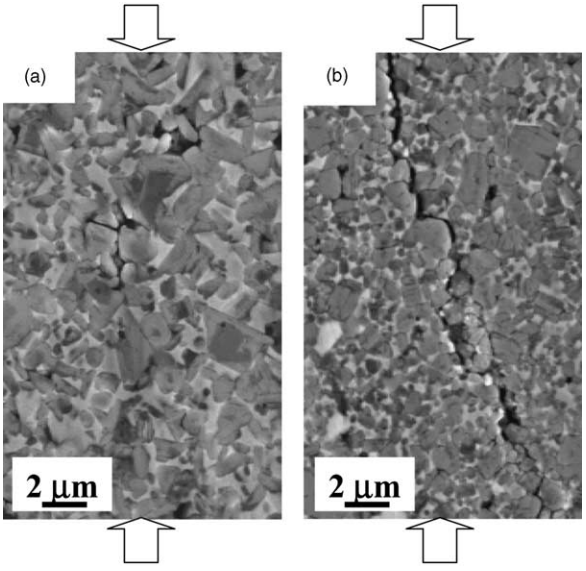

Fig. 4. SEM micrographs of the high-temperature damage in LPS SiC processed in: (a) Ar atmosphere and (b) N_2 atmosphere. The σ_e–% ε_e conditions are denoted by triangles in Fig. 3. The arrows denote the loading direction.

Fig. 4(a) and (b) are representative SEM micrographs of the high-temperature damage in Ar–LPS SiC and N_2–LPS SiC, respectively; the corresponding σ_e–%ε_e points are marked by triangles on Fig. 3. In Ar–LPS SiC, the damage is distributed in nature and it is characterized by the presence of short, disconnected cracks, which appear to have nucleated at interfaces and/or cavities. In contrast, the damage in N_2–LPS SiC is characterized by a single dominant crack running along the loading axis.

4. Discussion

We have demonstrated that sintering atmosphere (Ar or N_2) exerts a strong influence on the room- and high-temperature mechanical properties of the resulting LPS SiC ceramics.

With regards to room-temperature Hertzian indentation response, we saw that Ar–LPS SiC is more "quasi-ductile" (Fig. 2). This is due to a combination of the elongate nature of the SiC grains (Fig. 1) and the presumably weaker SiC–YAG interfaces in Ar–LPS SiC. Earlier work has clearly demonstrated that these microstructural ingredients produce "quasi-ductility" in ceramics, where shear-faulting occurs along the weak, elongated interfaces beneath the indenter.[3,4,25] This is also consistent with the relatively lower hardness in Ar–LPS SiC ($H = 17.6 \pm 0.3$ GPa), compared with N_2–LPS SiC ($H = 20.7 \pm 0.6$ GPa). The same microstructural ingredients also enhance the efficacy of the toughening mechanism crack-wake bridging, making those ceramics tougher.[2,26] This is borne out by the fact that Ar–LPS SiC has a higher toughness ($K_{IC} = 3.3 \pm 0.1$ MPa $m^{1/2}$), compared with N_2–LPS SiC ($K_{IC} = 2.2 \pm 0.1$ MPa $m^{1/2}$) with equiaxed SiC grains and presumably stronger SiC-YAG interfaces. In a previous study it was demonstrated that N_2-atmopshere sintering of LPS SiC results in the incorporation of nitrogen in the intergranular phase of N_2–LPS SiC.[19] It is believed that this results in the stronger SiC–YAG interfaces in N_2–LPS SiC.

A comparison of Figs. 1 and 4 reveals that shapes and sizes of the SiC grains in both materials are preserved during high-temperature deformation. This lack of grain deformation indicates that transport of point defects (Nabarro-Herring or Coble creep mechanisms) do not play a role here. This is not unreasonable because solid-state diffusion in SiC is expected to be very slow at the moderate temperature of 1400 °C.[27,28] Thus, it is argued that the high-temperature deformation of LPS SiC is based on grain-boundary sliding, which in turn is controlled by the deformation of the intergranular phase. In this context, internal friction measurements have shown that the incorporation of nitrogen in the intergranular phase of N_2–LPS SiC makes that phase highly viscous at high temperatures.[19] Thus, it is logical that N_2–LPS SiC is resistant to high-temperature deformation to a greater extent compared with Ar–LPS SiC, before the ultimate compressive strength is reached (Fig. 3).

Since grain boundary sliding does not appear to be accommodated by diffusive creep, cavitation and cracking are found to occur in both LPS SiC materials. In the case of Ar–LPS SiC, the damage was found to be more distributed (Fig. 4a), which could be the result of the relatively "softer" intergranular phase. Catastrophic failure requires the coalescence of the cavities/cracks into a single crack spanning the entire specimen. However, the elongate nature of the SiC grains in Ar–LPS SiC is likely to hinder the coalescence, resulting in the high strain-to-failure in Ar–LPS SiC (%$\varepsilon_F \sim 11.4$). The damage in N_2–LPS SiC, on the other hand, is less distributed due to the "harder" intergranular phase. Furthermore, the equiaxed SiC grains are likely to be less effective in offering resistance to damage coalescence, resulting in the lower strain-to-failure in N_2–LPS SiC (%$\varepsilon_F \sim 6$).

5. Summary

At room temperature, the equiaxed-grained microstructures and the nitrogen-containing "strong" intergranular phase in N_2–LPS SiC make this material less "quasi-ductile" under Hertzian indentation. This also makes N_2–LPS SiC harder and more brittle. In contrast, Ar–LPS SiC with its elongated-grained microstructures and "weak" interfaces is more "quasi-ductile", softer, and tougher. At high temperature, the equiaxed-grained

microstructures and the more viscous intergranular phase impart N_2–LPS SiC with higher deformation-resistance, higher ultimate compressive strength, but lower strain-to-failure. Ar–LPS SiC, on the other hand, has lower deformation resistance, lower ultimate compressive strength, but higher strain-to-failure, all due to the elongated-grained microstructure and less viscous intergranular phase devoid of nitrogen.

Acknowledgements

This work was supported by the Ministerio de Ciencia y Tecnología (Government of Spain) and the Fondo Europeo de Desarrollo Regional (FEDER) under grant No. CICYT MAT 2001-0799. The authors also thank financial support from FEDER under grant No. UNEX00-23-013. We are grateful to Dr. P. Miranda for helpful discussions and comments.

References

1. Suzuki, K. and Sasaki, M., Pressureless sintering of silicon carbide. In *Fundamental Structural Ceramics*, ed. S. Somiya and R. C. Bradt. Terra Scientific Publishing Company, Tokyo, Japan, 1987, pp. 75–87.
2. Padture, N. P., In situ-toughened silicon carbide. *J. Am. Ceram. Soc.*, 1994, **77**, 519–523.
3. Padture, N. P. and Lawn, B. R., Toughness properties of a silicon carbide with in situ-induced heterogeneous grain structure. *J. Am. Ceram. Soc.*, 1994, **77**, 2518–2522.
4. Lawn, B. R., Padture, N. P., Cai, H. and Guiberteau, F., Making ceramics "ductile". *Science*, 1994, **263**, 1114–1116.
5. Lee, S. K. and Lee, C. H., Effects of α-SiC versus β-SiC starting powders on microstructure and fracture-toughness of SiC sintered with Al_2O_3–Y_2O_3 additives. *J. Am. Ceram. Soc.*, 1994, **77**, 1655–1658.
6. Mulla, M. A. and Krstic, V. D., Mechanical properties of β-SiC pressureless sintered with Al2O3 additions. *Acta Metall. Mater.*, 1994, **42**, 303–308.
7. Kim, Y.-W., Mitomo, M., Emoto, H. and Lee, J. G., Effect of intital α-phase content on microstructural and mechanical properties of sintered silicon carbide. *J. Am. Ceram. Soc.*, 1998, **81**, 3136–3140.
8. Nader, M., Aldinger, F. and Hoffmann, M. J., Influence of the α/β-SiC phase transformation on microstructural development and mechanical properties of liquid phase sintered silicon carbide. *J. Mater. Sci.*, 1999, **34**, 1197–1204.
9. Sigl, L. S., Thermal conductivity of liquid phase sintered silicon carbide. *J. Eur. Ceram. Soc.*, 2003, **23**, 1115–1122.
10. Sigl, L. S. and Kleebe, H.-J., Core/rim structure of liquid-phase-sintered silicon carbide. *J. Am. Ceram. Soc.*, 1993, **76**, 773–776.
11. Krstic, V. D., Optimization of mechnical properties in SiC by control of the microstructure. *Mater. Res. Soc. Bull.*, 1995, **20**, 46–48.
12. Kim, Y.-W., Mitomo, M. and Hirotsuru, H., Microstructural development of silicon carbide containing large seed grains. *J. Am. Ceram. Soc.*, 1997, **80**, 99–105.
13. Ye, H., Pujar, V. V. and Padture, N. P., Coarsening in liquid-phase-sintered α-SiC. *Acta Mater.*, 1999, **47**, 481–487.
14. Kim, Y.-W., Mitomo, M. and Zhan, G.-D., Mechanism of grain growth in liquid-phase-sintered β-SiC. *J. Mater. Res.*, 1999, **14**, 4291–4293.
15. Jensen, R. P., Leucke, W. E., Padture, N. P. and Wiederhorn, S. M., High-temperature properties of liquid-phase-sintered α-SiC. *Mater. Sci. Eng.*, 2000, **A282**, 109–114.
16. Xu, H., Bhatia, T., Deshpande, S. A., Padture, N. P., Ortiz, A. L. and Cumbrera, F. L., Microstructural evolution in liquid-phase-sintered SiC: I, effect of starting SiC powder. *J. Am. Ceram. Soc.*, 2001, **84**, 1578–1584.
17. Deshpande, S. A., Bhatia, T., Xu, H., Padture, N. P., Ortiz, A. L. and Cumbrera, F. L., Microstructural evolution in liquid-phase-sintered SiC: II, effect of planar defects and seeds in the starting powder. *J. Am. Ceram. Soc.*, 2001, **84**, 1585–1590.
18. Kim, Y.-W. and Mitomo, M., Fine-grained silicon carbide ceramics with oxynitride glass. *J. Am. Ceram. Soc.*, 1999, **82**, 2731–2736.
19. Ortiz, A. L., Bhatia, T., Padture, N. P. and Pezzotti, G., Microstructural evolution in liquid-phase-sintered SiC: III, effect of nitrogen-gas sintering atmosphere. *J. Am. Ceram. Soc.*, 2002, **88**, 1835–1840.
20. Guiberteau, F., Padture, N. P. and Lawn, B. R., Effect of grain size on hertzian contact damage in alumina. *J. Am. Ceram. Soc.*, 1994, **77**, 1825–1831.
21. Lawn, B. R., *Fracture of brittle solids*, 2nd ed. Cambridge University Press, Cambridge, UK, 1993.
22. Lawn, B. R., Indentation of ceramics with spheres: a century after hertz. *J. Am. Ceram. Soc.*, 1998, **81**, 1977–1994.
23. Padture, N. P., Hertzian contacts. In *Encyclopaedia of materials: science and technology*, ed. R. W. C. K.H.J. Buschow, M. C. Flemings, B. Ilschner, E. Kramer and S. Mahajan. Pergamon Press, New York, NY, 2001.
24. deWith, G. and Parren, J. E. D., Translucent $Y_3Al_5O_{12}$ ceramics: mechanical properties. *Solid State Ionics*, 1985, **16**, 94–97.
25. Lee, S. K., Wuttiphan, S. and Lawn, B. R., Role of microstructure in hertzian contact damage in silicon nitride: I, mechanical characterization. *J. Am. Ceram. Soc.*, 1997, **80**, 2367–2381.
26. Li, C.-W., Lee, D.-J. and Lui, S.-C., R-curve behavior and strength of in-situ reinforced silicon nitride with different microstructures. *J. Am. Ceram. Soc.*, 1992, **75**, 1777–1785.
27. Hon, M. H. and Davis, R. F., Self-diffusion of C-14 in polycrystalline beta-SiC. *J. Mater. Sci.*, 1979, **14**, 2411–2421.
28. Hon, M. H., Davis, R. F. and Newbury, D. E., Self-diffusion of Si-30 in polycrystalline beta-SiC. *J. Mater. Sci.*, 1980, **15**, 2073–2080.